AFRL-AFOSR-VA-TR-2019-0035

Multiscale Experiments and Modeling of Dynamic Energetic Material Failure including Stochastic Interfaces

Caglar Oskay
VANDERBILT UNIVERSITY

12/14/2018
Final Report

Air Force Research Laboratory
AF Office Of Scientific Research (AFOSR)/ RTA1
Arlington, Virginia 22203
Air Force Materiel Command

REPORT DOCUMENTATION PAGE

Form Approved
OMB No. 0704-0188

1. REPORT DATE *(DD-MM-YYYY)*	2. REPORT TYPE	3. DATES COVERED *(From - To)*
25-02-2019	Final Performance	15 Apr 2015 to 14 Sep 2018

4. TITLE AND SUBTITLE
Multiscale Experiments and Modeling of Dynamic Energetic Material Failure including Stochastic Interfaces

5a. CONTRACT NUMBER

5b. GRANT NUMBER
FA9550-15-1-0202

5c. PROGRAM ELEMENT NUMBER
61102F

6. AUTHOR(S)
Caglar Oskay, Ibrahim Gunduz, Vikas Tomar

5d. PROJECT NUMBER

5e. TASK NUMBER

5f. WORK UNIT NUMBER

7. PERFORMING ORGANIZATION NAME(S) AND ADDRESS(ES)
VANDERBILT UNIVERSITY
110 21ST AVENUE S STE 937
NASHVILLE, TN 37203-2416 US

8. PERFORMING ORGANIZATION REPORT NUMBER

9. SPONSORING/MONITORING AGENCY NAME(S) AND ADDRESS(ES)
AF Office of Scientific Research
875 N. Randolph St. Room 3112
Arlington, VA 22203

10. SPONSOR/MONITOR'S ACRONYM(S)
AFRL/AFOSR RTA1

11. SPONSOR/MONITOR'S REPORT NUMBER(S)
AFRL-AFOSR-VA-TR-2019-0035

12. DISTRIBUTION/AVAILABILITY STATEMENT
A DISTRIBUTION UNLIMITED: PB Public Release

13. SUPPLEMENTARY NOTES

14. ABSTRACT
The proposed research aims to generate the fundamental knowledge base that specifically focuses on the effect of the variability of the material properties (especially interface properties) and mesoscale morphology on the dynamic response and hot spot formation in heterogeneous energetic materials. To achieve this aim, this research: (1) experimentally characterized and quantified the interfacial dynamic properties and their variability at the length scale of the meso- and microstructure; (2) establish the mesoscale structureproperty relationships and sensitivities that characterize the dynamic behavior in the presence of uncertainties. The research focused on the HMX-HTPB and AP-HTPB material systems

15. SUBJECT TERMS
energetic materials, mesoscale modeling, interfaces

16. SECURITY CLASSIFICATION OF:			17. LIMITATION OF ABSTRACT	18. NUMBER OF PAGES	19a. NAME OF RESPONSIBLE PERSON
a. REPORT	b. ABSTRACT	c. THIS PAGE			SCHMIDT, MARTIN
Unclassified	Unclassified	Unclassified	UU		19b. TELEPHONE NUMBER *(Include area code)* 703-588-8436

Standard Form 298 (Rev. 8/98)
Prescribed by ANSI Std. Z39.18

Project Final Report

Project Title: Multiscale Experiments and Modeling of Dynamic Energetic Material Failure including Stochastic Interfaces

Principal Investigators: Caglar Oskay, Vanderbilt University. Email: caglar.oskay@vanderbilt.edu. Phone: (615) 343-0583; Vikas Tomar, Purdue University. Email: tomar@purdue.edu. Phone: (765) 494-3423; Emre Gunduz, Purdue University. Email: igunduz@purdue.edu. Phone: (765) 494-0066.

Award Number: FA9550-15-1-0202

Program Manager: Dr. Martin Schmidt

Progress Reporting Period: April 15, 2017– September 14, 2018.

Overall Period of Performance: April 15, 2015– September 14, 2018.

Project Objectives:

There has been no change in the objectives of the project.

Status of Effort:

In the last half year of this project, the planned activities continued in both the experimental and computational tasks outlined in the original proposal, resulting in successful conclusion of the research. All activities performed directly support and in line with those proposed in the original project proposal. To achieve the objectives of the project in terms of numerical modeling and experimental characterizations, the accomplishments within the last six months of the project (during the no-cost-extension period) include the following:

1. Implemented and verified a fully three-dimensional crystal plasticity model to describe the dynamic response of polycrystalline β-HMX particles;
2. Performed global sensitivity analysis to elucidate the effect of monoclinic elasticity tensor components on the variability of the dynamic response of the polycrystal β-HMX specimen subjected to impact loading;
3. Analyzed the discrepancy between the local and global sensitivity of elastic coefficients on the plastic work in polycrystalline mesoscale specimens subjected to dynamic loads;
4. Performed sensitivity analysis to elucidate the effects and relative roles of various slip mechanisms and dislocation density evolution on the dynamic response of polycrystal β-HMX specimen;
5. Analyzed the discrepancy between the local and global sensitivities of various plastic deformation mechanisms on the maximum temperature rise in the polycrystal specimens subjected to dynamic loads;
6. Used a nanoscale dynamic impact experiment to obtain the constitutive model for bulk HTPB, AP as well as the HTPB-AP interface. A strain rate dependent power law viscoplastic model was fitted to the measured stress, strain and strain rate. It was observed that the interface constitutive behavior can be altered by adding a binding agent;

7. The interface delamination experiment under a quasi-static tensile loading combined with an in-situ MRS technique was used to obtain a cohesive zone model parameters for HTPB-AP interface. A tensile test was performed on a single particle edge crack sample with and without binding agent until failure. Crack propagation along the interface was monitored and the corresponding interface cohesive energy was obtained from the load displacement curve. Local stress near the interface during loading was obtained from MRS. It was observed that the interface strength increases with the addition of a binding;
8. Proposed a novel experimental setup based on impact simulations done for a single particle HTPB-AP sample. It was found that in order to measure interface level shock initiation, a direct interface impact set up was most appropriate. Also, an in-situ stress measurement was required. A laser induced particle impact combined with MRS was used to measure the shock viscosity at an interface. It was shown to be effective in measuring the interface level shock viscosity for both type of samples. The interface shock viscosity as a function of strain rate obtained from the current experiment was found to be qualitatively comparable with shock viscosity of different materials found in literature;
9. Thermal conductivity of HTPB-AP interface was obtained using Raman thermometry and was used for the evaluation of temperature change in the overall microstructure. Thermal conductivity for the HTPB-AP interface was found to be equal to 0.16 W/m.K and that for HTPB-AP-Tepanol was equal to 0.175 W.m.K;
10. The experimentally obtained material properties were then used in a cohesive finite element method framework and the model was validated against experimental observation available in literature;
11. Impact induced temperature rise, for an idealized HTPB-AP EM microstructure consisting of circular AP particles, was simulated considering viscoplastic, frictional and shock viscosity induced dissipation. It was observed that the interface shock viscosity leads to a decrease in the viscoplastic dissipation and the maximum temperature within the microstructure. It was also observed that the hot-spot density decreases with increasing shock viscosity. It was proposed that in order to predict the impact induced deformation behavior and the corresponding temperature rise in an EM microstructure, interface level properties should be considered in the model;

In the past three and a half years, this research resulted in 11 journal and proceeding articles (8 published, and 3 nearing submission). In addition, the outcomes of this research were presented in 11 conferences.

Accomplishments/New Findings:

Polycrystal Plasticity Simulations of HMX Specimen

The sensitivity analysis framework that was developed earlier in this project was previously applied on analysis of inelastic deformation processes within HMX single crystal, the interfacial separation behavior between elastic inclusion and polymeric binder under dynamic loads, and to assess morphological sensitivities. The crystallographic slip on slip systems within HMX crystals significantly contribute to the interfacial thermo-mechanical state as well as the material heterogeneity in a tightly packed energetic material. The contributions stem from the stress redistributions and material hardening/softening near the interfaces as a function of plastic

deformation, intra-particle plastic heat generation (adiabatic under impact/shock loads), as well as possible intragranular fracture and associated processes.

In the current period, we focused on extending the sensitivity analysis framework and investigating the role of plastic processes on the overall and interfacial behavior in *polycrystal* energetic particles (β-HMX) under impact loading. This builds on the work performed in the previous reporting period, which verified and validated the crystal plasticity model in the context of single crystal simulations.

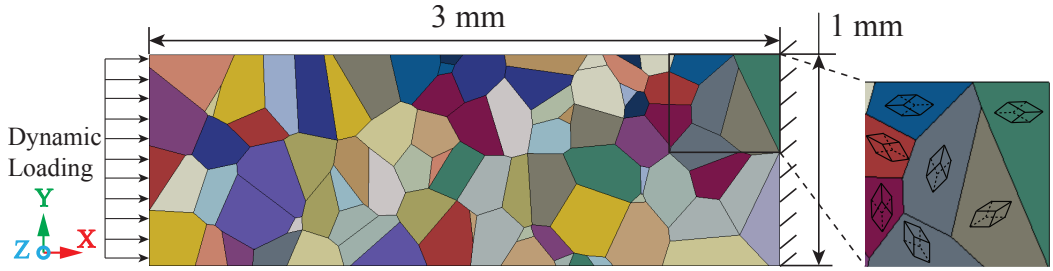

Figure 1: Polycrystal specimen geometry and experimental settings. Each particle represents a single crystalline. Random orientations are assigned to particles.

Plastic deformations in polycrystalline β-HMX mesostructures is of interest in view of the fact that the dynamics response of these materials is significantly affected by the stress and deformation heterogeneities at the crystal interfaces. The low crystal symmetry and the presence of multiple and potentially interacting plastic deformation results in complex response features under dynamic loads. In this research, we focused on the construction of representative polycrystalline β-HMX mesostructures and gaining the ability to perform polycrystalline simulations, which are in turn used in sensitivity analyses described below.

Mesoscale morphology characteristics such as the grain size distribution, orientation distribution and others significantly affect the response of energetic materials [1]. Figure 1 shows the geometry, morphology, loading and boundary conditions, as well as the discretization of the mesostructure considered in this study. The size of the numerical specimen is 3 mm x 1 mm that is made of 91 single crystals with random orientations sampled from uniform random orientation distribution. The size of the grains are sampled from a bimodal particle size distribution shown in Fig. 2 The mesostructure is subjected to the displacement controlled impact loading (250 /s) from the left edge of the specimen. The geometry is modeled as a quasi 2-D domain with three dimensional discretization constrained in the third (out of plane) direction with a single set of elements along the thickness direction. The mesoscale particle size probability distribution of

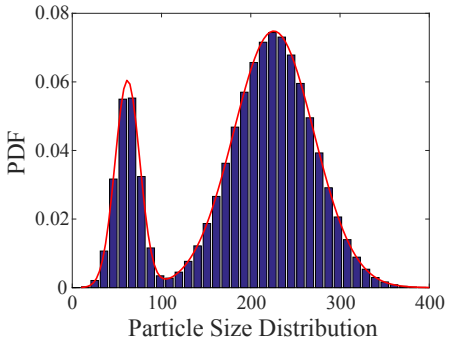

Figure 2: Bimodal particle size distribution. For the first normal distribution $N(\mu_1, \sigma_1)$, the weight $w = 0.2$, mean $\mu_1 = 61.8\,\mu m$, variance $\sigma_1 = 13.9\,\mu m$. For the second normal distribution $N(\mu_2, \sigma_2)$, mean $\mu_2 = 225.7\,\mu m$, variance $\sigma_2 = 44.9\,\mu m$.

β-HMX polycrystalline is constructed according to the available experimental data and numerical investigations available in the open literature [2-7].

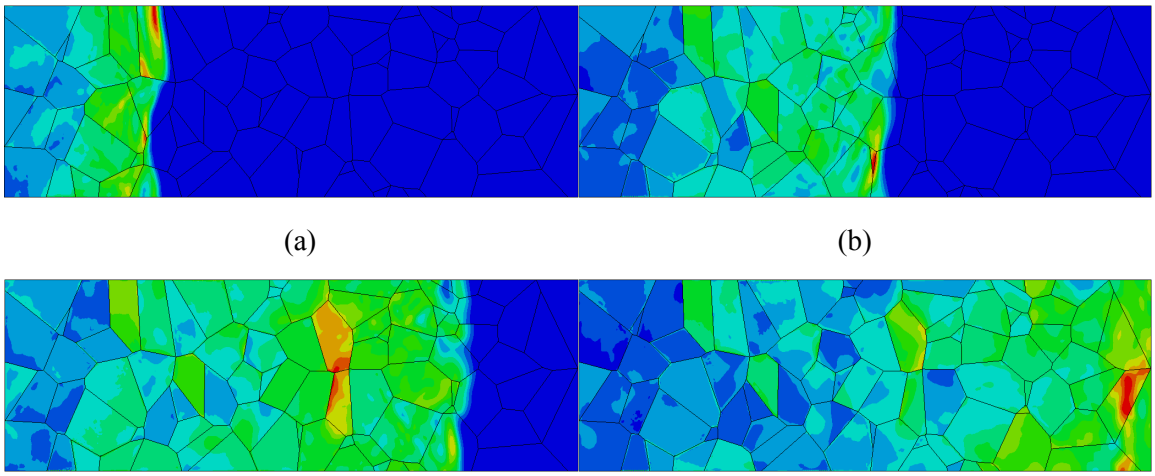

Figure 3: Von Mises stress contours at (a) $t = 0.2\ \mu s$, (b) $t = 0.5\ \mu s$, (c) $t = 0.75\ \mu s$, and (d) $t = 0.4\ \mu s$. The loading on the left hand side is $250\ m/s$. All model parameters, including elastic constants and plastic properties, remain the same with the parameters in Ref. [8].

Figure 3 illustrates the stress contours as the stress wave progresses through the specimen in a representative dynamic simulation. Local stress concentrations are apparent particularly along grain boundaries and triple junctions. The dislocation density generation and annihilation continuously drive local increase or decrease of the material strength, slip and plastic work in a complex fashion. Evolution of dislocation density distribution over the specimen is shown in Fig 4. The misorientation between adjacent grains leads to concentration of dislocations along grain boundaries and triple junctions.

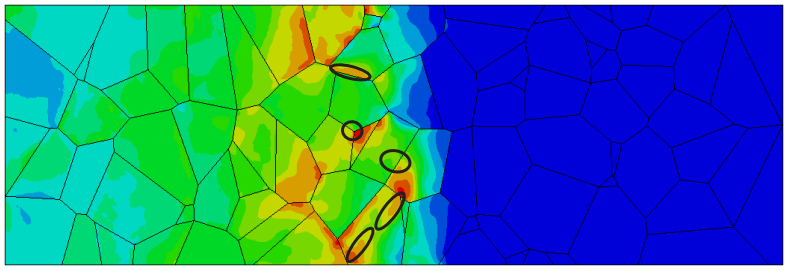

Figure 4: Dislocation density contour at $t = 0.55\ \mu s$. All model parameters remain the same with the parameters in Ref. [8].

The primary response function of interest is the peak temperature within the domain, which represents the most critical dissipative state across the mesostructure. In what follows, the mesostructural morphology is fixed and we focus on the analysis of the effects of elastic and plastic properties of the polycrystal.

Elastic Coefficients Sensitivity Analysis

The sensitivity of elastic coefficients of HMX polycrystal specimen with respect to heat generation is investigated under a displacement-controlled impact load at the LHS of the specimen. Ranges of the thirteen independent elasticity coefficients, which fully defines the monoclinic anisotropic properties, are estimated through the available experimental measurements and molecular simulations of β-HMX monoclinic crystal. As in the case of the single crystal investigations, four coefficients - C_{11}, C_{35}, C_{22}, C_{46} - are taken as constants and excluded from sensitivity studies. C_{33}, C_{44}, C_{55}, C_{66}, C_{12}, C_{23}, C_{15} and C_{25} are regarded as variables. The sensitivity analysis framework developed in this project has been used to assess the global sensitivity of the elasticity coefficients.

Approximately 2,000 forward mesoscale simulations are performed with parameters randomly sampled based on stratified sampling to serve as training dataset for the surrogate model. Following the surrogate model development, 140,000,000 model predictions were made using the surrogate to construct the output distributions.

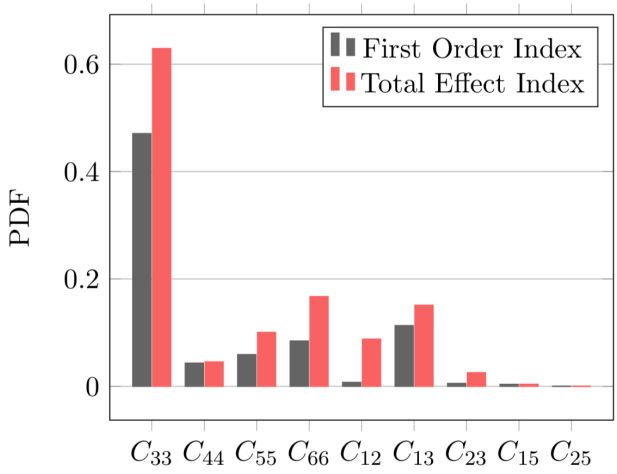

Figure 5: Sensitivity indices generated with 144 million prediction samples.

Figure 5 shows the global sensitivity indices for the elastic parameters. The plot clearly indicates that C_{33} is the most sensitive parameter under the applied impact loading. C_{33} is the out-of-plane stiffness and the corresponding high sensitivity is due to the confinement effect induced by the bonding condition employed in the out-of-plane direction. Shear coefficients of C_{55}, C_{66}, C_{12} and C_{13} exhibit relatively high sensitivity, with the remainder of the parameters to exhibit a small contribution to temperature rise.

Figure 6 demonstrates the sensitivity of the nine elastic constants (displayed as probability distributions) computed using the OAT method. In the OAT method, the sensitivity of a single parameter is computed by sampling that parameter from the range of values probed in the study, while keeping all other parameters fixed at their mean values. OAT therefore provides *local* variability of the response as a function of the parameter. C_{13} and C_{66} separately generate the largest temperature variations (~ 11 K) even though they are far less sensitive compared with C_{33} across the parameter subspace investigated in this study. Separately varying the parameter C_{15}, C_{25}

and C_{44} does not produce significant temperature rise (< 3 K), which is consistent with the corresponding low sensitivity indices in Fig. 5.

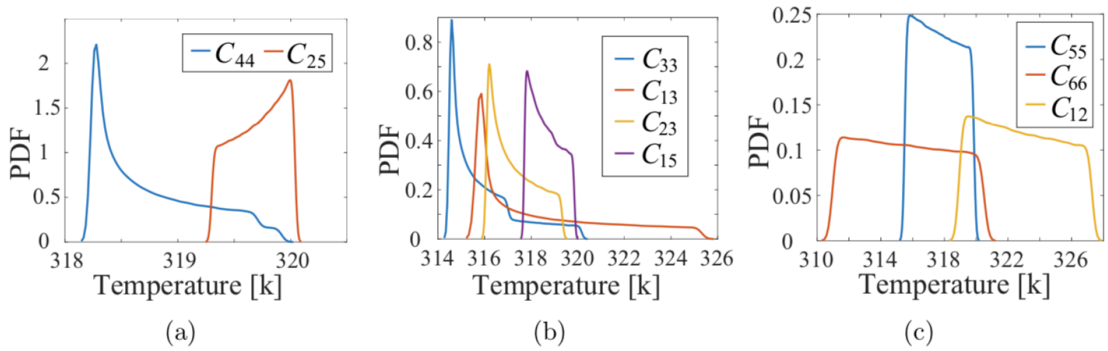

Figure 6: Temperature probability distribution resulted by the uncertainty of the individual elastic coefficient for polycrystal specimen.

The variation of the peak temperature over $C_{33} - C_{66}$ plane is shown in Fig. 7. This two-parameter sensitivity figure demonstrates the potential interactions between the most consequential parameters. Similar to the single crystal case, the plot indicates a convex shape with varying C_{66} for fixed C_{33} and a linear variation with C_{33} for a fixed C_{66}. In the present case, the curvature does vary with the value of C_{33}, which indicates some interactive effects between the two most influential parameters.

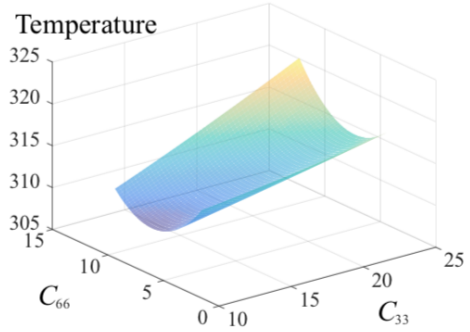

Figure 7: Temperature surface over $C_{33} - C_{66}$ plot.

Plastic Deformation Mechanisms Sensitivity Analysis

The sensitivity analyses have been performed to assess the relative roles of the plastic deformation mechanisms in the dynamic response of the polycrystalline mesostructure. The parameters that describe the crystal plasticity are considered variable, whereas the elasticity parameters are held constant, in order to construct the surrogate model, we performed approximately 3,000 CPFE simulations. The sensitivities were assessed based on 170,000,000 prediction points using the surrogate model.

Compared with the elastic constants, identification of appropriate parameter subspaces for plastic behavior is more challenging. This is due to the fact that different models available in the literature employ different internal state variables and evolution forms to describe the slip and strength evolution and that relatively small number of studies focused on accurate characterization of these parameters. The current crystal plasticity model consists of 16 parameters to describe the slip evolution by thermal activation ($\dot{\gamma}_{wo}^{\alpha}$, c_G, p, q, ζ), slip evolution by phonon drag ($\dot{\gamma}_{ro}^{\alpha}$, D_{ro}, θ_o), hardening evolution (g_o, s) adiabatic temperature evolution (c_V, η) and dislocation density

evolution (n_1, n_2, n_3, ρ_0). In what follows, we particularly focus on the investigation of the phonon drag, thermal activation and dislocation density evolution mechanisms. Eight parameters ($\dot{\gamma}_{wo}^{\alpha}$, c_G, $\dot{\gamma}_{ro}^{\alpha}$, D_{ro}, ρ_0, n_1, n_2, n_3) are considered as variables in the sensitivity analysis studies below.

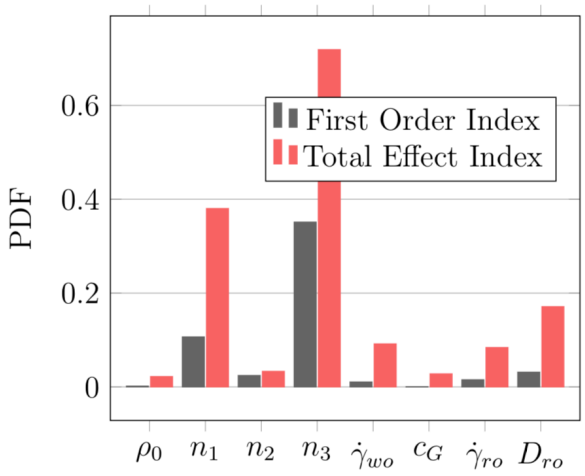

Figure 8: Sensitivity indices generated with 128 million prediction samples.

The results of the sensitivity indices (Fig. 8) are consistent with those from the single crystal analyses (results discussed in the previous report) that the dislocation evolution (particularly n_1 and n_2) along with phonon drag mechanisms primarily describe the plastic deformation and dissipation processes that occur under the applied dynamic loading. The distribution functions computed based on the OAT approach (Fig. 9) also indicate that, while the overall contributions and variabilities differ from those computed based on the global sensitivity analysis, the effects of phonon drag and dislocation density evolution are dominant. The key dislocation density evolution parameters that describe the generation and annihilation terms interact in a nonlinear fashion to describe the overall dissipative response and consequent temperature rise in the mesostructure, as shown in Fig. 8.

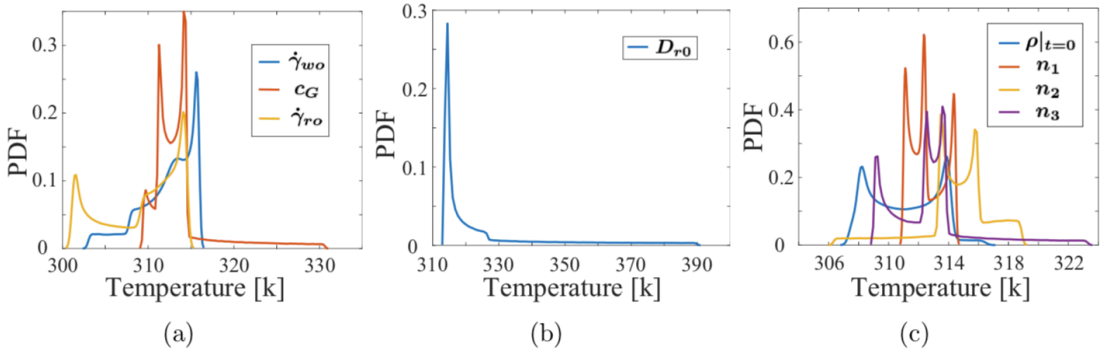

Figure 9: Temperature probability distribution resulted by the uncertainty of the individual plastic parameter for polycrystal specimen.

The variation of the peak temperature over $n_1 - n_3$ plane is shown in Fig. 10. In the polycrystal case, n_3 is more sensitive than n_2, while in the single crystal case that we have reported before n_2

significantly influence the dislocation annihilation which results in large temperature rise. The plot indicates a convex shape with varying n_3 for fixed n_1 and a linear variation with n_1 for a fixed n_3. In the present case, the curvature vary with the value of n_1, which indicates some interactive effects between the dislocation generation and annihilation process.

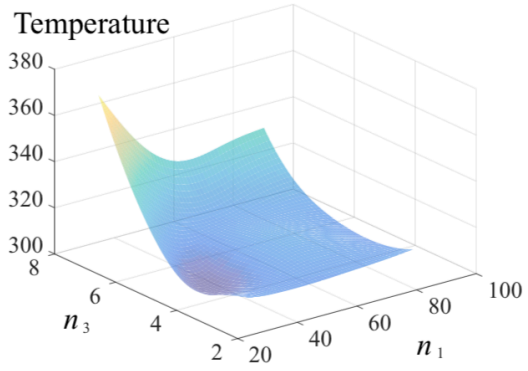

Figure 10: Temperature surface over $n_1 - n_3$ plane.

Constitutive Model for HTPB, AP and Interface

The constitutive material model and the cohesive zone model parameters were obtained from the experiments. A strain-rate dependent stress-strain law was obtained using a nanoscale dynamic impact experiment [1]. The stress-strain data obtained from the impact tests was fit to a viscoplastic power law model to define the constitutive behavior of the material. The viscoplastic model parameters for HTPB, AP and interface are shown in Table 1 [9].

Table 1: Constitutive model parameters for bulk and interface [9]

Parameter	χ (MPa)$^{-n}$	m	n
HTPB	0.54	-0.18	1.8
AP	3.7E10	-9.8	5.9
HTPB-AP Interface	1.0E5	-5.0	2.5
HTPB-AP-Tepanol Interface	1.0E4	-4.2	2.0

Cohesive Zone Model for HTPB, AP and Interface

In this work, an in-situ mechanical Raman Spectroscopy tests, as proposed by Prakash et al. [9], were performed in order to obtain the cohesive zone parameters. Cohesive zone parameters for bulk HTPB, AP and different interfaces are given in Table 2.

Table 2: Cohesive zone parameters of bulk and interface [9]

Material/Interface	Cohesive Strength (MPa)	Critical Displacement (mm)	Cohesive Energy (N/mm)
HTPB	0.8	0.5	0.2
AP	$2x10^3$	$5x10^{-3}$	5.0
HTPB-AP Interface	1.1	0.12	0.065

HTPB-AP-Tepanol Interface	2.91	0.11	0.16

Experimental Measurement of Interface Shock Viscosity

Shock viscosity is the ratio of the maximum stress to the applied strain rate. In order to obtain the shock viscosity, direct measurement of localized stress and strain rate is required. In the previous report it was shown that for interface shock viscosity, a direct interface impact setup is required. In this section the required experimental setup and the measurement techniques are described.

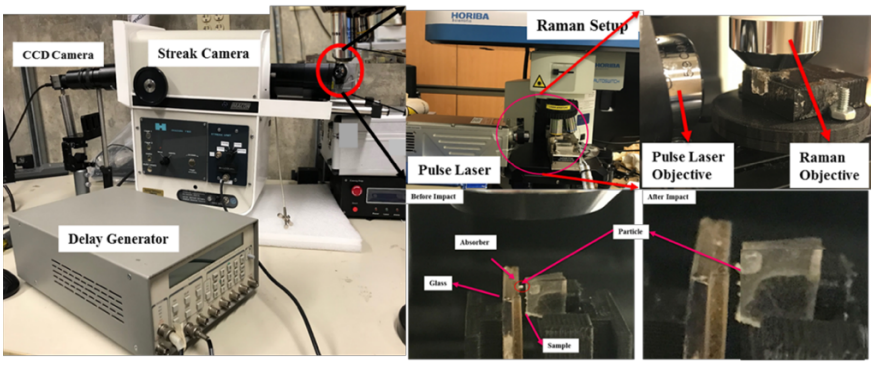

Figure 11: Experimental Setup for shock viscosity measurement.

Shock viscosity, η, is given by,

$$\eta = \frac{\sigma}{\dot{\varepsilon}} \tag{1}$$

where, σ is the maximum stress that occurs in the material across the shock wave and $\dot{\varepsilon}$ is the strain rate applied. In the current setup, Fig. 11, a pulse laser setup is used to accelerate a Si particle that precisely impact HTPB-AP interfaces at a velocity ranging from 1048 m/s to 1468 m/s. The velocity of the accelerated particles, *V*, is measured using a streak camera and the strain rate is calculated as,

$$\dot{\varepsilon} = \frac{\mathrm{V}}{\mathrm{h}}. \tag{2}$$

Here, *h* is the thickness of the sample. A local, in-situ stress at the interface where the impact occurs, is measured using MRS as explained earlier in section-2. Figure 12 (a) shows schematic of the particle impact experiment. A pulse laser (1064 nm, 2.5 mJ pulse energy and 9 ns pulse width by Opto-engine LLC) is focused on a glass substrate, on which an HTPB substrate is attached. A Si spherical particle of approximately ~1 μm diameter (procured from Alfa Aesar) is placed on the HTPB substrate layer. When the laser is focused on the glass, HTPB layer absorbs the energy and transfers it to the particle which then flies with a certain velocity toward the sample.

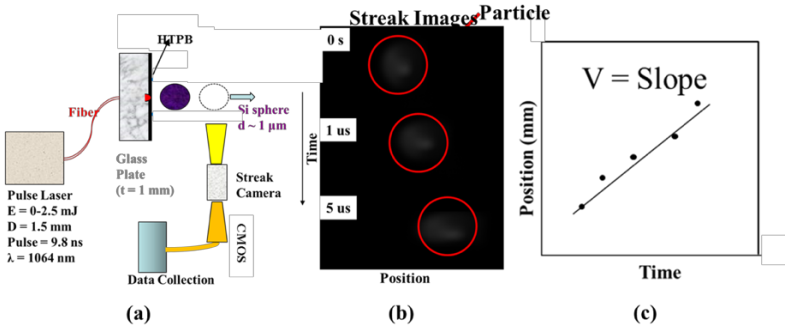

Figure 12: (a) Schematic of pulse laser induced particle impact and velocity measurement, (b) Streak images of particles and (c) velocity measurement from the streak images.

As shown in Fig. 12 (a), a high speed streak camera (IMACON 790) is used to collect the images of particle flying towards the sample. The camera is continuously triggered by a delay generator (DG 535) and a CMOS camera attached with a zoom lens (Navitar 700). The images acquired by the CMOS camera is automatically saved on a computer using Thorcam software. Streak images of the particle, Fig. 12 (b), represents particle position as a function of time which is used to obtain the velocity V of the particle as the slope of the position vs. time line as shown in Fig. 12 (c). This procedure is repeated for different values of the laser pulse energy for the same size of particles in order to obtain different strain rates for precise impact of particles at HTPB-AP interfaces.

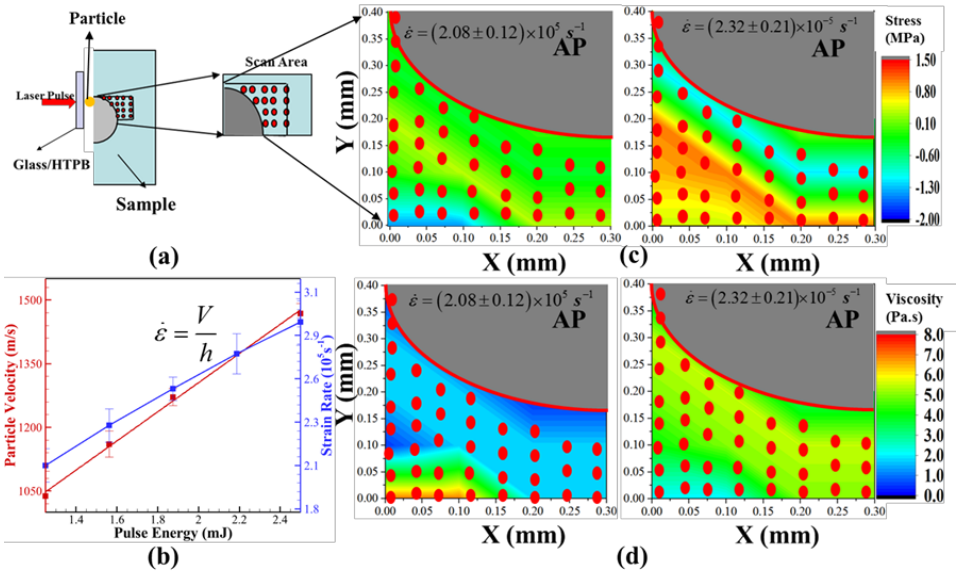

Figure 13: (a) Representative HTPB-AP impact sample, (b) particle velocity and strain rate at different pulse energy, (c) stress obtained in the scan area using MRS and (d) shock viscosity in the scan area for HTPB-AP-Tepanol sample.

As shown in Fig. 1 MRS setup is used in combination with the impact setup in order to in-situ measure stress at the HTPB-AP interfaces. Figure 3 (a) shows a representative interface impact setup of the HTPB-AP sample and the corresponding scan area near the interface. The velocity obtained from the streak camera images and the corresponding strain rates for increasing pulse energy used are shown in Fig. 3 (b). Figure 3 (c) shows the stress map obtained near the interface at two such strain rates. The interface shock viscosity is calculated using Eq. (1).

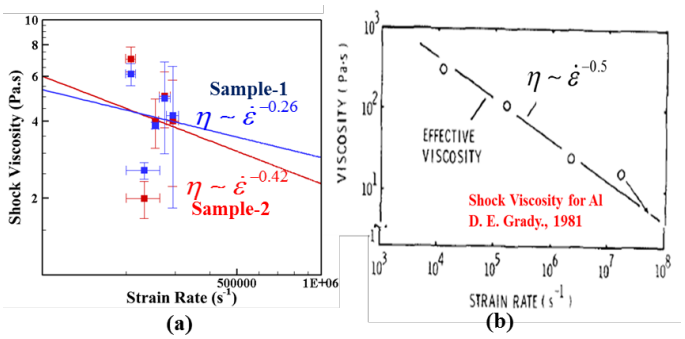

Figure 14: A qualitative comparison of (a) Interface shock viscosity measured using the current experimental setup for both samples (Sample-1 is without Tepanol and Sample-2 is with Tepanol) and (b) the shock viscosity measured for Al (Reprinted with permission from (D. E. Grady 1981 [10]). Copyright (2018) AIP Publishing).

Based on the maximum stress obtained from the stress map in Fig. 3 (c) and the corresponding strain rate, a plot of the interface shock viscosity with respect to the applied strain rate is obtained, Fig. 4 (a). For both samples, with and without the binding agent, the shock viscosity is found to be in the range of 2 to 6 Pa.s. Since there is no available measured value of interface shock viscosity, a qualitative comparison of the current trend of shock viscosity as a function of strain rate is performed with that of the shock viscosity obtained for Al, as shown in Fig. 4 (b). D. E. Grady [11] has reviewed shock behavior of several different materials, such as granular materials, composites, metals, etc., and have established an empirical power law relation between shock viscosity and the strain rate. However, the analysis used in these studies, to obtain shock viscosity, do not consider any local variation in the shock wave behavior because of the limitation in their experimental measurements. Also, in order to obtain shock viscosity, stress is calculated either from the shock Hugoniot relation or taken to be equal to the applied pressure [11]. These assumptions are not be valid in case of composite materials where impedance mismatch among constituent material will affect the shock wave propagation as well as the local stress. The current work focuses on measuring the interface stress and the corresponding shock viscosity. As can be seen in Fig. 4 (a), interface shock viscosity shows a clear variation as a function of chemical composition. Table 3 lists the value of shock viscosity for HTPB, AP and the HTPB-AP interface used in this work.

Table 3: Shock viscosity of bulk and interface.

	HTPB[12]	AP[13]	HTPB-AP Interface	HTPB-AP-Tepanol Interface
Viscosity (Pa.s)	1.5	30	4.8	6

Thermal Conductivity for HTPB-AP Interface

In order to model the thermal behavior of the HTPB-AP energetic material, thermal conductivity values of the individual constituents are needed. For the HTPB and AP phases, thermal conductivity values are readily available in literature. However, there are no available thermal conductivity values for the HTPB-AP interface. In this work, an in-situ MRS method is used to experimentally measure the thermal conductivity at HTPB-AP interface. Several researchers have

shown this method to be an effective and accurate tool in the temperature distribution measurement as well as the thermal conductivity measurement [14, 15]. In order to measure the temperature distribution around an interface, first a correlation between the changes in Raman shift due to known externally applied temperature needs to be obtained. The experimental setup to obtain the calibration relation between Raman shift and the temperature change is shown in Fig. 15 (a). The sample is mounted on a hot-stage where a temperature detector is attached to one end of the sample and the other end was heated using electric coils. An Ar+ laser beam (Modu-Laser Inc., UT) of wavelength 514.8 nm was directed at the sample as the sample was being heated. The backscattered laser beam was collected back by an objective and directed to a spectrometer (Acton SP2500; Princeton Instruments Inc., NJ). A low power laser beam (~5 mW) was used to measure the Raman shift so that the temperature change due to laser beam remains insignificant [15]. In this work, a correlation between the Raman shift of the CH_2 asymmetric stretching mode (Fig. 15 (b)) and the sample temperature was obtained. The Raman shifts at different temperatures were obtained as plotted in Fig. 15(c). A linear relationship between the Raman shift and the temperature change from the reference value of the sample was fitted to a linear relation, which is given by,

$$\Delta w = C\Delta T \tag{3}$$

where the value of C is obtained from the slope of the linear correlation curve in Fig. 15 (c), which is equal to 0.121 cm^{-1}/K. This calibration constant is then used to calculate the temperature change of the samples by measuring the change in Raman shift values.

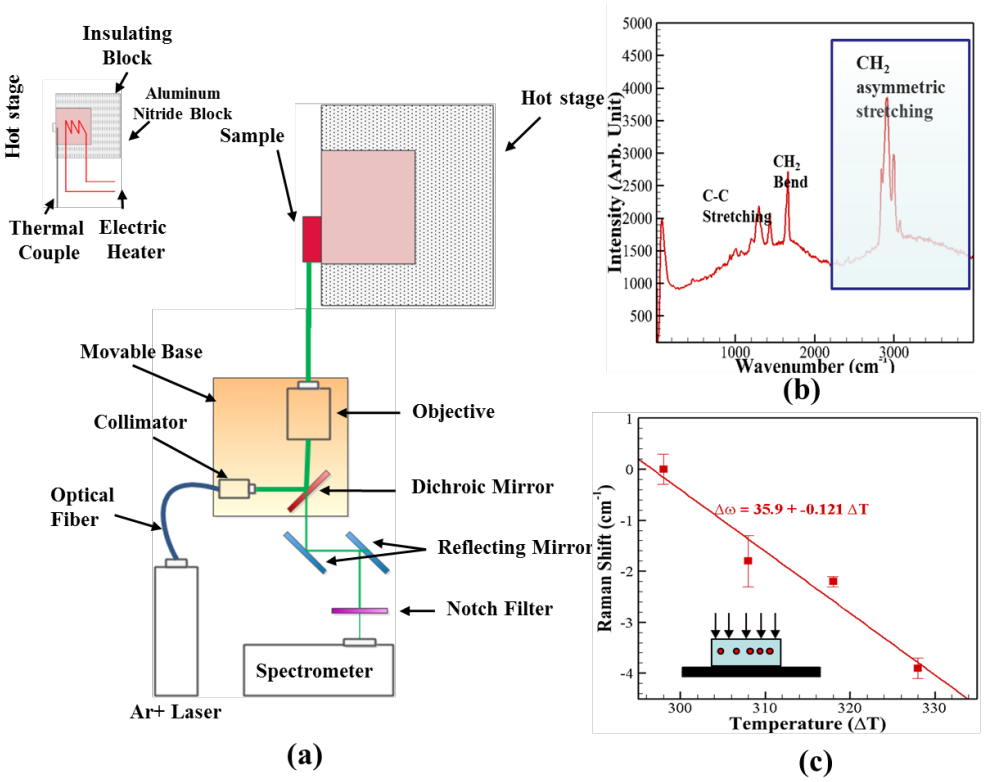

Figure 15: (a) Experimental set-up for Raman shift vs temperature change calibration, (b) a representative Raman spectra of HTPB and (c) calibration curve for Raman shift vs temperature change.

By measuring the laser energy absorbed by the sample and corresponding temperature increase of the laser spot on the sample, the thermal conductivity of the sample can be derived with a heat transfer model. It has been shown that the isothermal conditions can be assumed and the interface between sample and the substrate can be assumed to be hemispheric, if the thickness of the sample is more than one magnitude larger than the laser spot size. A Horiba Xplora Plus Raman spectroscope was used to measure the Raman shift during loading. A 532 nm wavelength laser was used with a laser power of 20 mW and the laser spot size (d) was found to be of approximately 1 µm. By measuring the laser power (P) and corresponding temperature change (ΔT) thermal conductivity of the sample can also be calculated using [7],

$$\kappa = \frac{2P}{\pi d \Delta T} \tag{4}$$

Using Eq. (3) for the temperature change in Eq. (4), the thermal conductivity can be written as,

$$\kappa = \frac{2PC}{\pi d \Delta \omega} \tag{5}$$

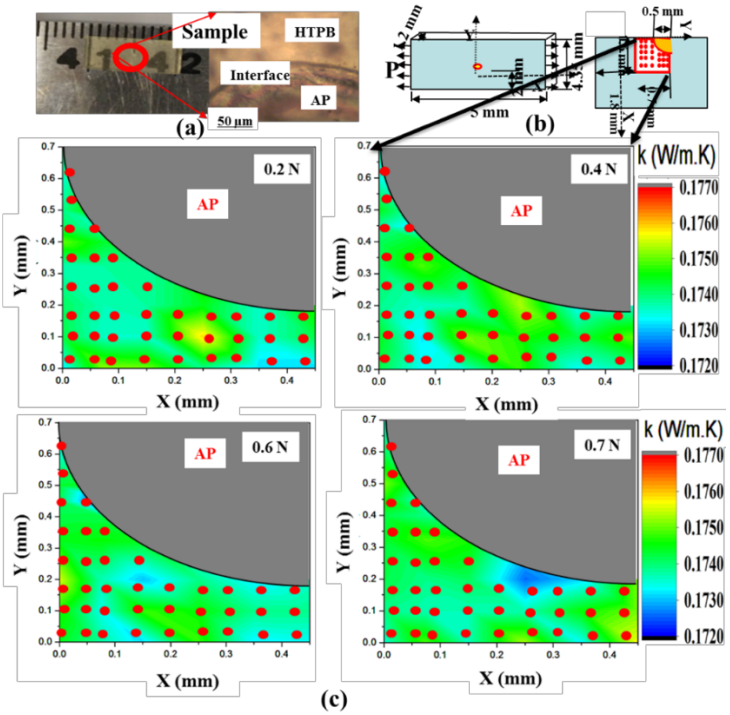

Figure 16: (a) HTPB-AP tensile sample, (b) sample dimensions, boundary conditions and the scan area and (c) thermal conductivity near the HTPB-AP-Tepanol interface.

In this work, a tensile load is applied to a single particle HTPB-AP sample as shown in Fig. 16 (a) and the change in Raman shift near the HTPB-AP interface in the scan area (Fig. 16 (b)) was obtained. Thereafter, Eq. (5) was used to calculate thermal conductivity of the scan area near the HTPB-AP interface. As can be seen from Fig. 16 (c) for different tensile load, a slight decrease in the thermal conductivity is observed. Thermal conductivity and heat capacity of the HTPB, AP and the HTPB-AP interface used in the simulation are given in Table 4. The value of heat capacity for the HTPB-AP interface was obtained as the average value of AP and HTPB phase values as suggested by Hu et al. [16].

Table 4: Thermal properties of HTPB, AP and the HTPB-AP Interface

	HTPB	AP	HTPB-AP Interface	HTPB-AP-Tepanol Interface
Thermal Conductivity (W/m.K)	0.28[17]	0.4[17]	0.16	0.175

Prediction of Local Temperature Rise using Cohesive Finite Element Method

In order to simulate the high strain rate dependent deformation and temperature rise behavior, cohesive finite element method (CFEM) is employed [9,18,19]. The finite element mesh for the modelled microstructure was generated with 'cross triangle' elements and cohesive surfaces at all element boundaries, as shown in Fig. 17. The rectangular mesh size for all models, which contains four 'cross triangle' elements each, was 1 μm, creating 250,000 elements in the domain.

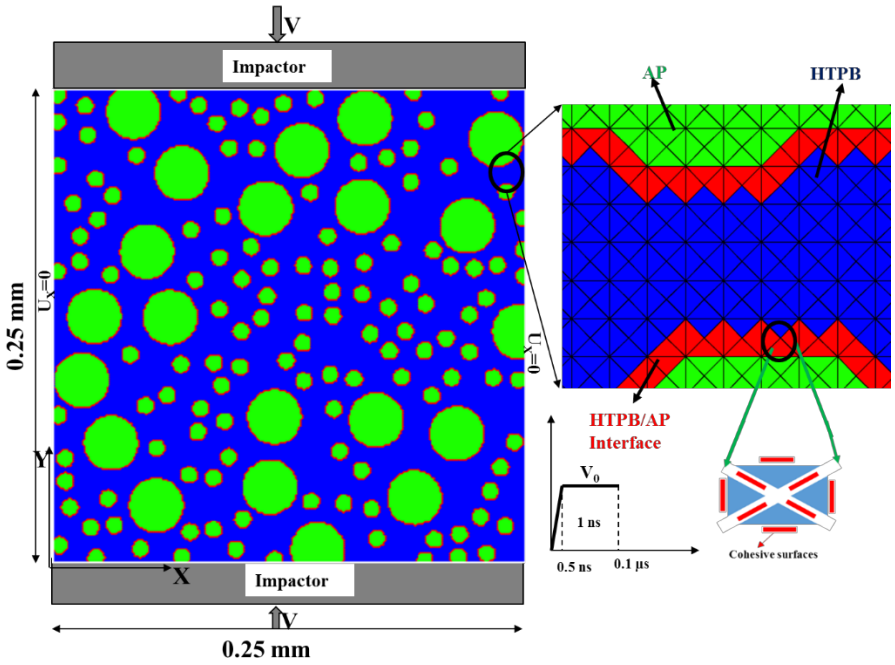

Figure 17: The finite element model of HTPB-AP microstructure (50% AP density) showing boundary conditions, and the mesh details as well as cohesive surfaces.

For the continuum elements, the viscoplastic constitutive model is used to govern the stress-strain relations while the irreversible bilinear cohesive law for tensile separation is used to govern the separation at the cohesive surfaces. The large deformation viscoplastic model has been described in an earlier work by the authors [19]. The Jaumann objective rate is used in the model and the rate of Cauchy stress tensor is given as,

$$\hat{\boldsymbol{\tau}} = \dot{\boldsymbol{\tau}} - \boldsymbol{W}\cdot\boldsymbol{\tau} + \boldsymbol{\tau}\cdot\boldsymbol{W} = \boldsymbol{C} : [\boldsymbol{D} - \boldsymbol{D}^{vp}]. \tag{6}$$

where $\boldsymbol{C}$ is the stiffness tensor. The flow rule for large deformation for an isotropic hardening solid, $\boldsymbol{D}^{vp}$ is given by,

$$D_{ij}^{vp} = \frac{\partial f}{\partial \tau_{ij}} \dot{\lambda} = \frac{3}{2\bar{\sigma}} \tau_{ij}^{'} \dot{\lambda}, \tag{7}$$

where, f is defined as the Mises yield function and $\dot{\lambda}$ is equal to an effective viscoplastic strain rate, given by,

$$\dot{\lambda} = \sqrt{\frac{2}{3} D_{ij}^{vp} D_{ij}^{vp}} = \dot{\bar{\varepsilon}}^{vp} = \frac{d\bar{\varepsilon}^{vp}}{d\bar{\sigma}} \dot{\bar{\sigma}}, \tag{8}$$

$$\bar{\sigma} = \sqrt{\frac{3}{2} \tau_{ij}' \tau_{ij}'}, \ \boldsymbol{\tau} = \boldsymbol{\tau}' + \boldsymbol{\tau}^{v} - pI, \tag{9}$$

where, $\boldsymbol{\tau}_{ij}^{v} = \eta D_{ij}$ [13] is the viscous stress, p is the pressure, and $\bar{\varepsilon}^{vp}$ is the effective viscoplastic strain and is given as [9],

$$\bar{\varepsilon}^{vp} = \chi \left(\dot{\bar{\varepsilon}}^{vp} \right)^{m} \left(\bar{\sigma} \right)^{n}. \tag{10}$$

The parameters in Eq. (10) are evaluated by fitting the data obtained from the dynamic impact experiment. Pressure is calculated from a polynomial form of the Mie-Gruneisen equation of state [19].

In order to prevent interpenetration of bulk elements, an acceleration correction term is used that is obtained based on a frictional cohesive contact model for large deformation impact simulation. As was shown in a previous work by the authors [19], the element penetration in this model is insignificant for the total time of the simulation. In order to identify the local temperature rise within the microstructure, a temperature increase from the reference temperature, $\Delta T = T - T_{ref}$, was calculated from [13],

$$T = \frac{e + e_f - e_c}{\rho c_p} \tag{11}$$

where, T_{ref} = 298 K, e is the internal energy density of the system, e_f is the frictional dissipation energy density, e_c is the cold compression energy density [13], ρ is the material density and c_p is the heat capacity at constant pressure. The rate of heat generation (h) by the frictional forces at the bulk element interfaces is distributed among the contacting bulk elements based on ratio of heat supply [20].

The CFEM simulation model described in [9,19], is used in predicting the effect of interface shock viscosity on the overall microstructure dependent impact behavior and temperature increase due to impact in multi-particle HTPB-AP sample (Fig. 17). Strain rate dependent power law viscoplastic stress-strain model, as given in Table 1, was used for HTPB, AP and the HTPB-AP interface [9]. The cohesive zone model parameters, as given in Table 2, obtained experimentally through mechanical Raman spectroscopy, were used for modeling cohesive separation behavior [21]. The interface shock viscosity is shown in Table 3 [19]. Thermal conductivity and heat capacity of the HTPB, AP and the HTPB-AP interface used in the simulation are given in Table .

The value of heat capacity for the HTPB-AP interface was obtained as the average value of AP and HTPB phase values as suggested by Hu et al. [16].

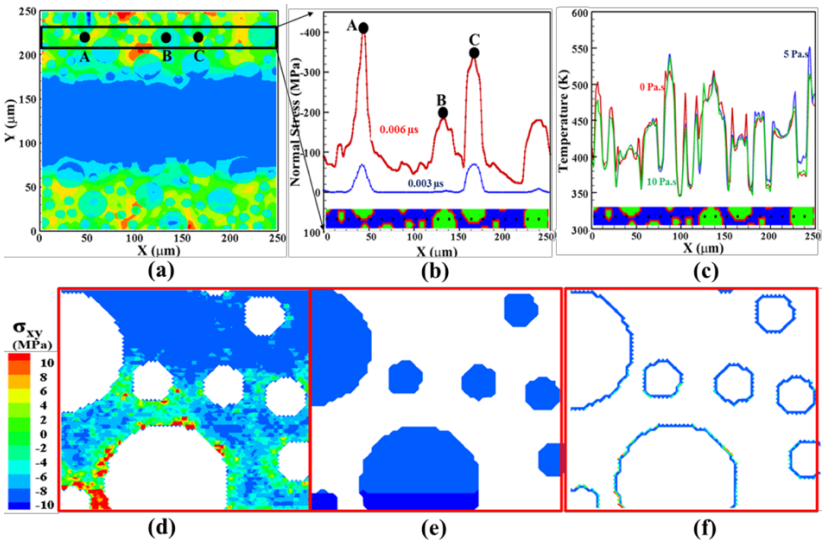

Figure 18: Selected cross-section in the HTPB-AP microstructure. (b) Normal stress profile at different time steps and (c) temperature as a function of interface shock viscosity along the selected cross-section. Shear stress map in the near position *A* in (d) HTPB, (e) AP and (f) the HTPB-AP interface.

The impact induced local temperature rise in an idealized HTPB-AP EM microstructure (Fig. 17), with circular AP particles, were simulated. The circular AP particles had radii varying from 5μm to 15 μm with 50% area fraction. In order to understand the effect of individual constituents HTPB, AP and the HTPB-AP interface) of the microstructure, first the impact behavior of the microstructure was analyzed for a strain rate of 100,000 s^{-1}. The shock pressure waves are transmitted, without significant reflection, through the interface of HTPB and the AP particles when the particle density is high, i.e. when the amount of bulk HTPB phase separating the particles is small. This can be explained by observing the stress profile along a cross-section with varying AP particle distribution. The normal compressive stress distribution along a selected cross-section is shown in Fig. 18. The specific section, Fig. 18(a), is chosen because of the continuously varying local particle size and density distribution. The position marked A, corresponds to the position at the HTPB-AP interface phase where two particles are separated only by 2 μm which is covered by HTPB-AP interface phase. The position marked B, corresponds to the position inside an AP particle. The position marked C, corresponds to the position inside an AP particle but close to the HTPB-AP interface. As shown in Fig. 18(b), maximum stress occurs close to the HTPB-AP interfaces around larger AP particles (position A and C). It is observed that initially (at time 0.003 μs) only the interface around large AP particles where particles are closely packed, experiences a higher stress concentration. This is due to the increase in the interaction between AP particles and the stress concentration at the HTPB-AP interfaces as was also reported earlier by authors [19] for a single particle HTPB-AP sample. As time progresses, the normal stress inside the particle (position B) increases but remains below the value at the HTPB-AP interface (position A or C). Temperature profile, in Fig. 18 (c), shows that the temperature jumps to a higher value in the HTPB-AP interface phase and drops again inside the HTPB and AP phase. Also, as the interface shock viscosity increases, the temperature decreases significantly at the HTPB-AP interface positions where particle density is low. However, near the HTPB-AP interface phase, where the particle interaction is high, effect of interface shock viscosity is low. Also, as can be observed from

Fig. 18 (c), temperature shows a decrease in the value with increasing interface shock viscosity when transitioning from HTPB to AP phase due to the presence of the HTPB-AP interface phase. This occurs due to the fact that the energy dissipation at the shock front increases with the interface shock viscosity which leads to a decrease in the temperature.

Shear stresses distribution near a HTPB-AP interface region where particles are in close vicinity is shown in Fig. 18. Shear stress in the bulk HTPB (Fig. 18(d)) and AP (Fig. 18(e)) are negligible and are concentrated in the HTPB-AP interface phase only, Fig. 18(f). This is because the interface boundaries can act as a source as well as a barrier to the shear wave, depending on where the shear localization starts. In this case, since the localization starts at the interface, as shown in Fig. 18 (d), the shear stress remains concentrated along the interface itself and does not propagate further into the bulk, Fig. 18(d-f). This shear localization behavior then results into an increased viscoplastic and frictional dissipation near the HTPB-AP interface region which leads to a local increase in the temperature.

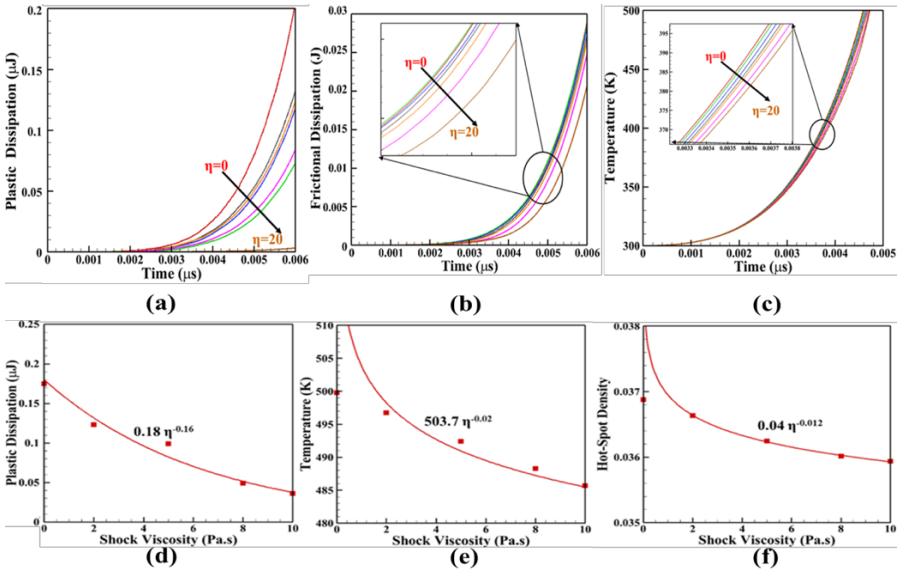

Figure 19: (a) Plastic dissipation history, (b) frictional dissipation history and (c) maximum temperature history in the HTPB-AP microstructure. Effect of interface shock viscosity on (d) plastic dissipation, (e) maximum temperature and (f) the hot-spot density.

Temperature change in the microstructure is a function of the plastic and frictional heat dissipation as given in Eq. (11). The viscoplastic deformation was observed to have higher value within the HTPB-AP interface phase and the bulk HTPB near the interface than that in the AP, as was shown in Fig. 19. A plastic dissipation and frictional dissipation energy history as a function of interface shock viscosity is shown in Fig. 19 (a) and Fig. 19 (b) respectively. As shown, both energy dissipation decreases with increase in interface viscosity. This results in lower temperature increase as the interface shock viscosity increases as shown in Fig. 19 (c). It has also been discussed earlier, [11], that the effect of interface shock viscosity is to widen the interface shock front which leads to a decrease in the dissipation energy and the temperature near the interface.
Impact induced temperature may increase to or greater than a certain threshold value, within the microstructure, at several position simultaneously. A measure of such local temperature rise can be taken to be equal to the number of elements per unit area within the HTPB-AP microstructure which rises above a threshold temperature value. In this work, this number density is assumed to

be the 'hot-spot' density. In this work the maximum temperature for comparison is taken to be 500 K, which is the temperature after which AP phase change starts to occur. It is observed that the maximum temperature, within the microstructure, decreases by more than 20 K by adding interface shock viscosity in the model. This is in agreement with the effect of shock viscosity obtained by D. J. Benson [13] in a shocked granular HMX. Correspondingly, the hot-spot density in the microstructure also decreases. Fig. 9 (d-f) shows the plastic dissipation, the maximum temperature in the microstructure and the hot-spot density as a function interface shock viscosity. Fig. 19 (d-f), for comparison purposes, were plotted at the time step, when the maximum temperature, in the case of zero interface shock viscosity, reaches 500 K. It is to be noted that in the current work only 6% area fraction of the microstructure is modeled with HTPB-AP interface phase properties. The stress, dissipation energy and the temperature decrease in the microstructure was found to be significant and in order to predict the temperature increase accurately in EM composites, numerical simulation models should account for the shock viscosity and the effect of interfaces.

References

[1] X. Zhang, and C. Oskay, "Material and morphology parameter sensitivity analysis in particulate composite materials" in *Computational Mechanics*, 2018. 62(3): 543-561.

[2] D. B. Hardin, J. J. Rimoli, and M. Zhou, "Analysis of thermomechanical response of polycrystalline HMX under impact loading through mesoscale simulations" in *AIP Advances*, 2014. 4(9): 097136.

[3] A. R. Zamiri, and S. De, "Multiscale modeling of the anisotropic shock response of β-HMX molecular polycrystals" in *Interaction and multiscale mechanics*, 2011. 4(2): 139-153.

[4] X. Wang, Y. Wu, F. Huang, T. Jiao, and R. J. Clifton, "Mesoscale thermal-mechanical analysis of impacted granular and polymer-bonded explosives" in *Mechanics of Materials*, 2016. 99: 68-78.

[5] C. B. Skidmore, D. S. Phillips, S. F. Son, and B. W. Asay, "Characterization of HMX particles in PBX 9501" in *AIP Conference Proceedings*, 1998. 429(1): 579-582.

[6] P. J. Rae, H. T. Goldrein, S. J. P. Palmer, J. E. Field, and A. L. Lewis, "Quasi–static studies of the deformation and failure of β–HMX based polymer bonded explosives" in *Proceedings of the Royal Society of London A: Mathematical, Physical and Engineering Sciences*, 2002. 458(2019): 743-762.

[7] C. Zhang, Q. Peng, L. Wang, and X. Wang, "Thermal Sensitivity of HMX Crystals and HMX-Based Explosives Treated under Various Conditions" in *Propellants, Explosives, Pyrotechnics*, 2010. 35(6): 561-566.

[8] N. R. Barton, N. W. Winter, and J. E. Reaugh, "Defect evolution and pore collapse in crystalline energetic materials" in *Modelling and Simulation in Materials Science and Engineering*, 2009. 17(3): 035003.

[9] C. Prakash, et al., "Effect of interface chemistry and strain rate on particle-matrix delamination in an energetic material" in *Engineering Fracture Mechanics*, 2018. 191: 46-64.

[10] D.E. Grady, "Strain-rate dependence of the effective viscosity under steady-wave shock compression" in *Applied Physics Letters*, 1981. 38(10): 825-826.

[11] D.E. Grady, “Structured shock waves and the fourth-power law” in *Journal of Applied Physics*, 2010. 107(1): 013506.

[12] B. Florczak, “Viscosity Testing of HTPB Rubber Based Pre-binders” in *Central European Journal of Energetic Materials*, 2014. 11(4): 625-637.

[13] D.J. Benson and P. Conley, “Eulerian finite-element simulations of experimentally acquired HMX microstructures” in *Modelling Simul. Mater. Sci. Eng.*, 1999. 7: 333-354.

[14] M. Gan, V. Samvedi, and V. Tomar, “Raman Spectroscopy-Based Investigation of Thermal Conductivity of Stressed Silicon Microcantilevers” in *Journal of Thermophysics and Heat Transfer*, 2014. 29(4): 845-857.

[15] Y. Zhang, M. Gan, and V. Tomar, “Raman Thermometry Based Thermal Conductivity Measurement of Bovine Cortical Bone as a Function of Compressive Stress” in *Journal of Nanotechnology in Engineering and Medicine*, 2014. 5(2): 021003-021003.

[16] R. Hu, et al., “Experimentally-validated mesoscale modeling of the coupled mechanical–thermal response of AP–HTPB energetic material under dynamic loading” in *International Journal of Fracture*, 2016: 1-22.

[17] J. Zhang, S. Zhi, and B. Sun, “Estimation of thermophysical properties of solid propellants based on particle packing model” in *Science China Technological Sciences*, 2013. 56(12): 3055-3069.

[18] C. Prakash, I.E. Gunduz, and V. Tomar, “Interface Shock viscosity in Energetic material using Cohesive Finite Element Method” in *2018 AIAA/ASCE/AHS/ASC Structures, Structural Dynamics, and Materials Conference*. 2018, American Institute of Aeronautics and Astronautics.

[19] C. Prakash, I.E. Gunduz , and V. Tomar, “Experimental Interface Shock Viscosity Measurement in an Energetic Material Using Pulse Laser Induced Particle Impact Loading Combined With Mechanical Raman Spectroscopy”, *Manuscript Under preparation*, 2018.

[20] G.T. Camacho and M. Ortiz, “Computational Modeling of Impact damage in brittle materials” in *International Journal of Solids and Structures*, 1996. 33(20-22): 2899-2938.

[21] A.M. Olokun, et al. “Interface Chemistry Dependent Mechanical properties in Energetic Materials using Nano-scale impact experiment” in *2018 SEM Annual Conference*. 2018. Greenville, SC: Springer.

Personnel Supported:

Three graduate research assistants (GRA), a visiting researcher, in addition to the PIs have performed the research tasks of this project. Two GRAs have been supported directly from the project funds. The other personnel have been supported by other sources (identified below) but directly contributed to the execution of the project tasks.

Personnel supported in the last six months of the project are:

- Prof. Caglar Oskay is responsible for overseeing the execution of the overall research tasks as outlined above. He also serves as the doctoral dissertation advisor of the graduate research assistants involved in this project at Vanderbilt University.

- Prof. Vikas Tomar is responsible for overseeing the execution of the research tasks at Purdue University as outlined above. He also serves as the doctoral dissertation advisor of the graduate research assistants involved in this project.

- Chandra Prakash is a graduate research assistant at Purdue University working under supervision of both Drs. Tomar and Gunduz. He is responsible for executing the experimental and computational tasks being performed at Purdue University.

- Ayotomi Olokun is a graduate research assistant at Purdue University working under supervision of Dr. Tomar. She is responsible for executing the experimental and computational tasks being performed at Purdue University with emphasis on HMX.

- Xiaoyu Zhang is a graduate research assistant at Vanderbilt University supported by this project. In Year 3, he has been responsible for performing the numerical modeling aspects of the project, with particular emphasis on implementation of and analysis with the crystal plasticity model and employing the proposed sensitivity analysis framework to investigate parameter sensitivity.

Personnel contributing to the project in Years 1 and 2 are:

- Prof. Emre Gunduz is responsible for overseeing the execution of the research tasks at Purdue University in years 1 and 2. He also serves as the doctoral dissertation advisor of the graduate research assistants involved in this project.

- Ruize Hu is a graduate research assistant at Vanderbilt University partially supported by this project in Year 1. He was responsible for undertaking the computational model development, implementation and analysis for the HTPB-AP composites.

- Dr. Shuiwen Zhu was a visiting researcher at Vanderbilt University. He directly contributed to the objectives of the project during April 2015-March 2016 and was self-supported. He was responsible for undertaking the theoretical development and formulation of the reduced order multiscale modeling of viscoelastic composites with specific focus on HTPB-AP systems.

Publications:

- Chandra Prakash, Devendra Verma, Matthias Exner, Emre Gunduz, and Vikas Tomar, "Strain Rate Dependent Failure of Interfaces Examined via Nanoimpact Experiments" in *SEM Annual Conference Proceedings*, Orlando, FL, June 6-9, 2016.
- Ruize Hu, Chandra Prakash, Vikas Tomar, Michael Harr, I. Emre Gunduz and Caglar Oskay, "Experimentally-validated mesoscale modeling of the coupled mechanical-thermal response of HTPB-AP energetic material under dynamic loading", *International Journal of Fracture*, 203:277-298, 2017.
- Chandra Prakash, Devendra Verma, and Vikas Tomar, "Dynamic local vs. non-local properties of material interfaces", *Handbook of Nonlocal Continuum Mechanics for Materials and Structures*, Springer, ISBN 978-3-319-58729-5, 2017.

- Devendra Verma, Sudipta Biswas, Chandra Prakash, and Vikas Tomar, "Relating Interface Evolution with Interface Mechanics based on Interface Properties", *Journal of Materials* (TMS), 69:30–38, 2017.
- Chandra Prakash, Ibrahim Emre Gunduz, and Vikas Tomar, "Effect of Strain Rate and Interface Chemistry on Failure in Energetic Material Examined via Mechanical Raman Spectroscopy and Cohesive Finite Element Method", in *SEM Annual Conference Proceedings*, Indianapolis, IN, June 12-15, 2017.
- Chandra Prakash, I. Emre Gunduz, and Vikas Tomar, "Interface Shock viscosity in Energetic material using Cohesive Finite Element Method", *Proceedings of AIAA-SciTech Meeting*, Gaylord Palms, Kissimmee, Florida, Paper No. 273-MAT-7, January 8–12, 2018.
- Chandra Prakash, Caglar Oskay, Ibrahim Emre Gunduz, and Vikas Tomar, "Effect of interface chemistry and strain rate on particle-matrix delamination in energetic materials", *Engineering Fracture Mechanics*, 191:46-64, 2018.
- Xiaoyu Zhang and Caglar Oskay, "Material and Morphology Parameter Sensitivity Analysis in Particulate Material", *Computational Mechanics,* 62:543-561, 2018.
- Chandra Prakash, I. Emre Gunduz and Vikas Tomar, "Effect of the Interface Chemistry on the Interface Shock Wave Rise Time in an Energetic Material analyzed using the Cohesive Finite Element Method", submitted to *International Journal of Impact Engineering*.
- Ayotomi Olokun, Chandra Prakash, I. Emre Gunduz and Vikas Tomar, "Effect of Microstructure on the Failure Behavior of Energetic Materials due to Impact", submitted to *International Journal of Mechanical Sciences*.
- Xiaoyu Zhang and Caglar Oskay, "Crystal Properties, Kinematic Mechanisms and Morphology Parameters Sensitivity Analysis of β-HMX in Polymer-bonded Composite under Dynamic Loading", in-preparation for journal publication.

Interactions/Transitions:

(a) *Participation/presentations at meetings, conferences, seminars, etc.*

- Ruize Hu and Caglar Oskay, "Experimentally-validated mesoscale modeling of the coupled mechanical-thermal response of AP-HTPB energetic material under dynamic loading", *Engineering Mechanics Institute Conference*, Nashville, TN, May 22-25, 2016.
- Ruize Hu and Caglar Oskay, "Experimentally-validated mesoscale modeling of the coupled mechanical-thermal response of AP-HTPB energetic material under dynamic loading", *Poster Presentation at the Engineering Mechanics Institute Conference*, Nashville, TN, May 22-25, 2016.
- Devendra Verma and Vikas Tomar, "Strain Rate Dependent Failure of Interfaces in Glass/Epoxy and Energetic Materials At Nano-Microscale Via Dynamic Indentation", *Engineering Mechanics Institute Conference*, Nashville, TN, May 22-25, 2016.
- Chandra Prakash, Devendra Verma, Matthias Exner, Emre Gunduz, and Vikas Tomar, "Strain Rate Dependent Failure of Interfaces Examined via Nanoimpact Experiments", *SEM Annual Conference*, Orlando, FL, June 6-9, 2016.

- Caglar Oskay and Vikas Tomar participated in the “Mesoscale Modeling of Explosives Initiation Workshop” held in Livermore, CA, October 11-13, 2016.
- Ruize Hu and Caglar Oskay, "Experimentally-validated mesoscale modeling of the coupled mechanical-thermal response of AP-HTPB energetic material under dynamic loading", *ASME International Mechanical Engineering Congress & Exposition*, Phoenix, AZ, November 11-17, 2016.
- Chandra Prakash, Ibrahim Emre Gunduz, and Vikas Tomar, “Effect of Strain Rate and Interface Chemistry on Failure in Energetic Material Examined via Mechanical Raman Spectroscopy and Cohesive Finite Element Method”, *MACH Conference*, Annapolis, MD, April 4-7, 2017.
- Xiaoyu Zhang and Caglar Oskay, “Material Properties and Morphology Parameters Sensitivity Analysis in Energetic Materials”, *14th US National Congress on Computational Mechanics*, Montreal, Canada, July 17–20, 2017.
- Prakash, C., and Tomar, V., “Interface Chemistry and Strain Rate Effect on Fracture in Energetic Material Interfaces", *Materials Science & Technology*, Pittsburgh, PA, October 08-12, 2017.
- Xiaoyu Zhang and Caglar Oskay, “Material and Morphology Parameter Sensitivity Analysis in Polymer-Bounded Polycrystalline Energetic Materials”, *MACH Conference*, Annapolis, MD, April 4-6, 2018.
- Xiaoyu Zhang, Chandra Prakash, Vikas Tomar and Caglar Oskay, “Experimental and Computational Investigations of Interface Chemistry Dependence and Parameter Sensitivity of Dynamic Response and Fracture in Energetic Materials”, *Gordon Research Seminar* (Energetic Materials), Newry, ME, June 2-3, 2018.

(b) *Consultative and advisory functions to other laboratories and agencies, especially Air Force and other DoD laboratories. Provide factual information about the subject matter, institutions, locations, dates, and names(s) of principal individuals involved.*

- Caglar Oskay served as the subject matter expert during Summer 2016 and Summer 2017 at AFRL Structural Sciences Center. The PI frequently visited AFRL at the Wright Patterson Air Force Base. The PI conducted research in close collaboration with the in-house scientists and engineers (particularly Dr. Brian Gockel, Dr. Ravi Penmetsa and Dr. Ravi Chona) in developing and implementing physics-based, multi-scale, computational and analytical models for capturing the evolution of accumulating damage and forecasting structural life for aero-thermo-structures operating in combined extreme environments (coupled thermo-acousto-chemo-mechanical loading). This research enables long-term, reliable assessments of the durability and continued safe operation of designs that are proposed and/or developed for hypersonic air-breathing vehicles, space operating vehicles, reusable, single-stage to orbit space vehicles, and other like vehicles.

(c) *Technology Assists, Transitions, and Transfers. Describe cases where knowledge resulting from your effort is used, or will be used, in a technology application. Transitions can be entities in the DoD, other federal agencies, or industry. Briefly list the enabling research, the laboratory or company, and an individual in that organization who made use of your research.*

N/A

New discoveries, inventions, or patent disclosures:

An interface cohesive traction and interface fracture toughness measurement setup was established using Nanomechanical Raman Spectroscopy technique patented by Dr. Tomar's group.

Honors/Awards: List honors and awards received during the grant/contract period. List lifetime achievement honors such as Nobel Prize, honorary doctorates, and society fellowships prior to this effort:

Prof. Caglar Oskay (reporting accomplishments during the grant period. Other previous additional awards and fellowships skipped for brevity)

- *Chancellor Faculty Fellow (2016-2018)*
- *2017 ASME Fellow*

Prof. Vikas Tomar (reporting accomplishments during the grant period. Many previous additional awards and recognitions skipped for brevity)

- *2015 AIAA Associate Fellow*
- *2016 ASME Fellow*
- *2016 University Faculty Scholar at Purdue University*
- *2017 CT Sun Research Award from Purdue University*
- *2017 Chandra Prakash AAE Teaching Scholarship*